Supplementary Information for

High-entropy engineering for achieving linear-like behavior and superior energy storage in $Bi_{0.5}Na_{0.5}TiO_3$-based lead-free relaxor ferroelectrics

Jiangping Huang, Yu Zhang, Yue Pan, Xiuli Chen *, Xu Li *, Huanfu Zhou

Key Laboratory of New Processing Technology for Nonferrous Metal and Materials, Ministry of Education, Guangxi Key Laboratory of Optical and Electronic Materials and Devices, College of Materials Science and Engineering, Guilin University of Technology, Guilin, 541004, China

* Corresponding author, Email: cxlnwpu@163.com; lx100527@163.com

1. Structure characterizations

The phase structure and local structure evolution of all samples were characterized by X–ray powder diffraction (XRD, model X'Pert PRO; PA Nalytical, Almelo, The Netherlands) using Cu Kα radiation (λ = 0.15406 nm) and Raman(XDR) (XDR, Thermo Fisher Scientific, USA) tests, respectively. A scanning electron microscope (model GeminiSEM 300, OXIG, Oxfordshire, UK) was used to observe the microstructure of the specimens. The dielectric-temperature spectrum of the ceramics was measured using a precision impedance analyzer (Model 4294A, Hewlett–Packard Co, Palo Alto, CA) in the temperature range of 30 to 400°C with the heating rate of 2 °C min^{-1}. A simple parallel plate capacitor was fabricated for *P–E* loop testing (Ferroelectric Material Parameter Tester (RT66, Radiant Technologies, NM, USA)). Dielectric Charge Test System (model PK-DIS10012, PolyK Technologies, USA) was used to measure the charging/discharging properties, and a 10 kΩ overload resistance was used. To study the evolution of domain structures, Piezoresponse Force Microscope (PFM, MFP-3D, UK) is applied by Pt/Ir-coated conductive tips (Nanosensors, Neuchatel, Switzerland) with an AC tip voltage of 3 V in out-of-plane mode.

2 Phase-field simulations method for breakdown behavior of ceramics

Building on the phase-field breakdown model proposed by Hong et al. [1], here a scalar field $s(\mathbf{x}, t)$ is introduced to characterize the breakdown state of the 0.92BNBT-0.06NMS and 0.84BNBT-0.16NMS ceramics. In this model, the s ranges from 1 to 0, representing the intact state and the complete breakdown state, respectively. Herein, ε_r is a continuous function of the field variable s and can be expressed as [2, 3]:

$$\varepsilon(s) = \frac{\varepsilon_{intact}}{f(s) + \delta}, \tag{1}$$

where $f(s) = 4s^3 - 3s^4$, δ is a very small value. To quantitatively describe the dielectric breakdown

behavior, the $\varepsilon_r(0)$ of the matrix phase is set to 10/1 (the ratio of the grain to the grain boundary). For the ferroelectric polycrystalline ceramics in this study, the grain regions are considered to have pronounced ferroelectric properties. The corresponding ε_r is electric field dependent following Johnson's approximation [4]. For the grain boundary regions, the ε_r is approximately independent of the electric field. Therefore, the relationship between the dielectric constant of ceramic and the electric field can be expressed by the following formula :

$$\varepsilon_r(E) = \begin{cases} \varepsilon_g(0)/(1+kE^2)^{2/3}, & \text{the grain regions} \\ \varepsilon_{gb}(E), & \text{the grain boundary regions} \end{cases}, \tag{2}$$

where the parameter k is a material constant that is related to the Johnson's parameter β by $k = 3[\beta(\varepsilon_0\varepsilon_g(0)^3]$. The $\varepsilon_g(0)$, and $\varepsilon_{gb}(0)$ are the ε_r of grain and grain boundary regions at zero electric field, respectively. The theoretical model in this work is built by the dimensionless governing equation as follows [5]:

$$\begin{cases} \overline{\nabla}[\varepsilon_g(s)(1+\overline{k}\overline{\nabla}\overline{\phi}\cdot\overline{\phi})^{-\frac{1}{3}\overline{\nabla}\overline{\phi}}] = 0 \\ \dfrac{\partial s}{\partial \overline{t}} = -\dfrac{3\varepsilon_g'(s)}{4k}((1+\overline{k}\overline{\nabla}\overline{\phi}\cdot\overline{\nabla}\overline{\phi})^{\frac{2}{3}}-1) + f'(s) + \dfrac{1}{2}\overline{\nabla}^2 s \end{cases}, \text{ the grain regions}, \tag{3}$$

$$\begin{cases} \overline{\nabla}\cdot[\varepsilon_{gb}(s)\overline{\nabla}\overline{\phi}] = 0 \\ \dfrac{\partial s}{\partial \overline{t}} = -\dfrac{\varepsilon_{gb}'(s)}{2}\overline{\nabla}\overline{\phi}\cdot\overline{\nabla}\overline{\phi} + f'(s) + \dfrac{1}{2}\overline{\nabla}^2 s \end{cases}, \text{ the grain boundary regions}, \tag{4}$$

where the electric field vector $\boldsymbol{E}$ is related to the field of electric potential $\boldsymbol{\phi}(\mathbf{x}, t)$($\boldsymbol{E} = -\nabla\boldsymbol{\phi}$). Due to computational limitations, simulation is carried out in two-dimensional (2D) domains. The electric field concentrator is introduced to control the overall random defects. Eqs. (3) and (4) are applied to the solution of dimensionless unknown fields $\phi(\mathbf{x}, t)$and $s(\mathbf{x}, t)$.

3. Supplementary Figures

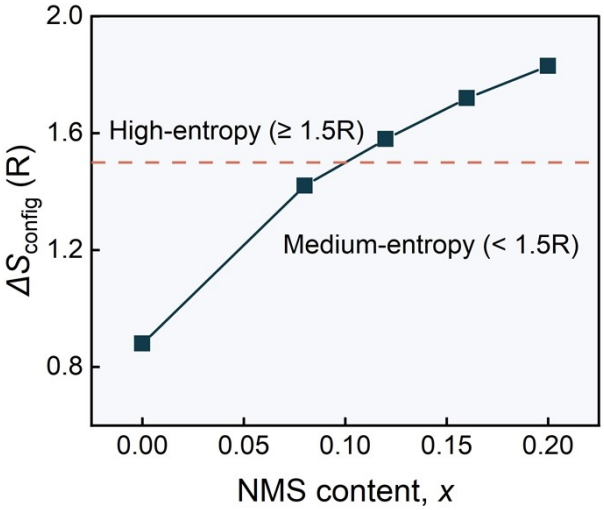

Figure S1 The configuration entropy (ΔS_{config}) for the (1-x)BNBT-xNMS ceramics.

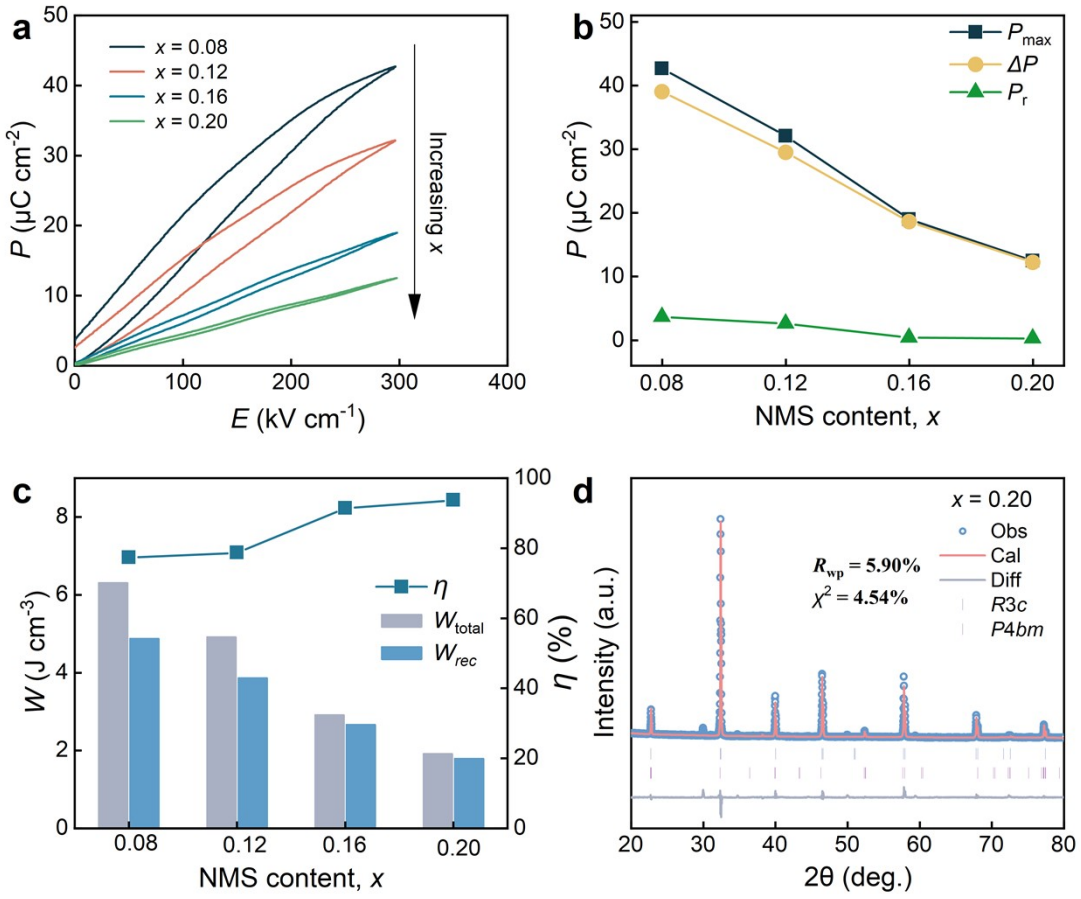

Figure S2 (**a**) Unipolar P-E hysteresis loop of (1-x)BNBT-xNMS ceramics under 300 kV cm^{-1} and (**b-c**) the corresponding changes in polarization and energy storage parameters. (**d**) Rietveld refinements for x = 0.20.

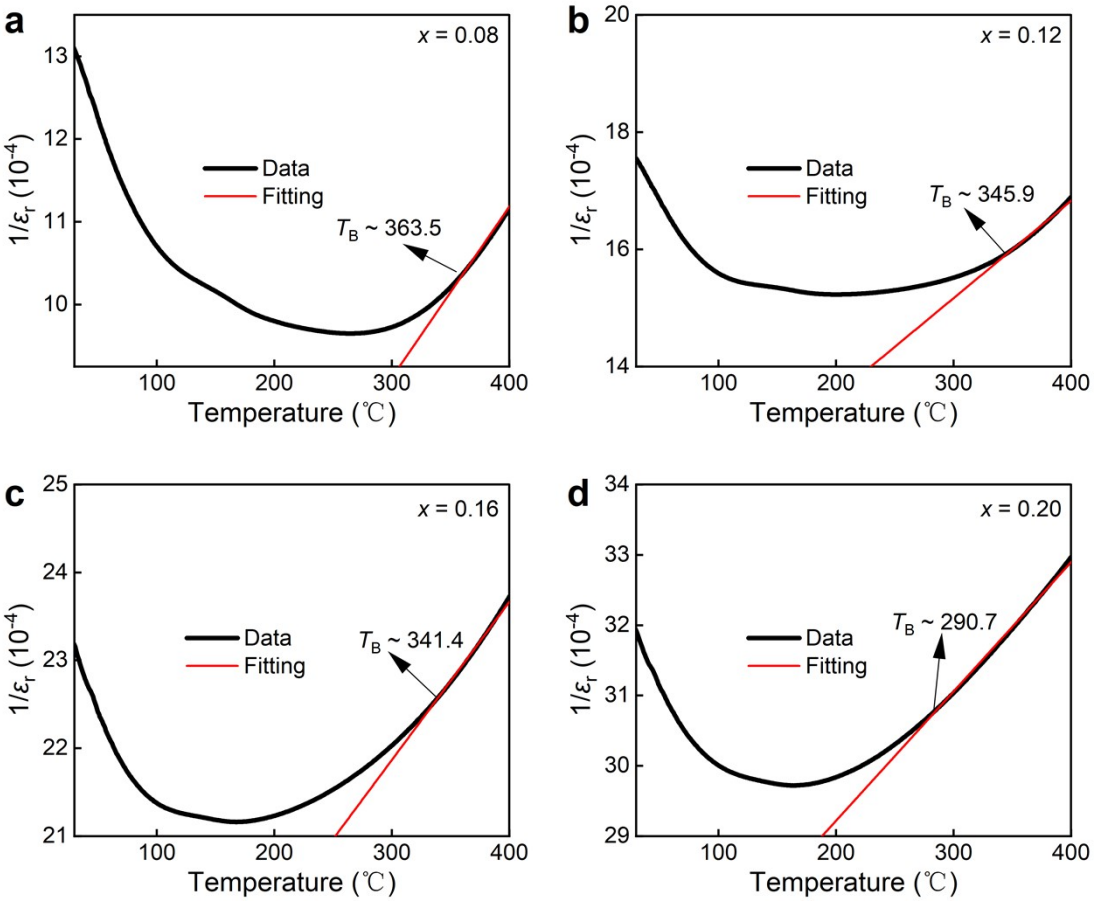

Figure S3 (**a-d**) Temperature dependence reciprocal of ε_r for (1-*x*)BNBT-*x*NMS ceramics at 10 kHz.

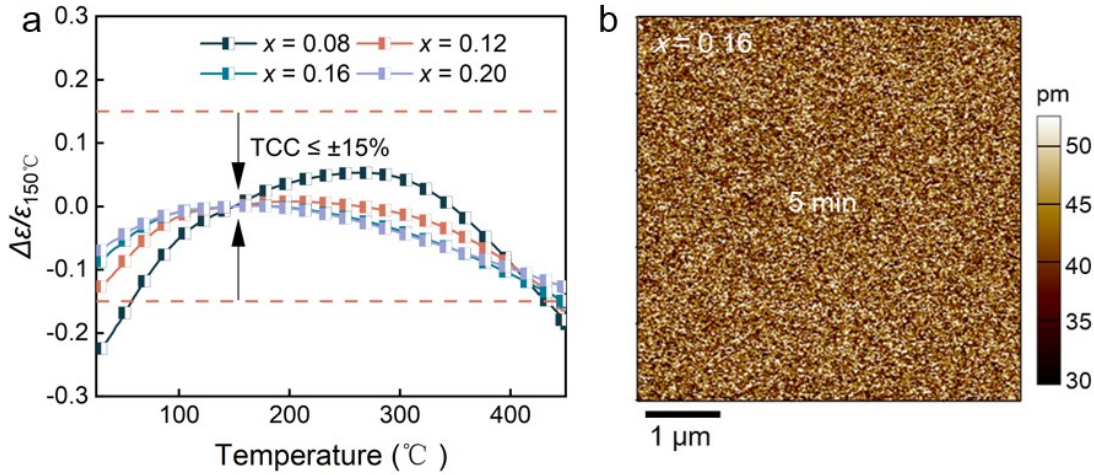

Figure S4 (a) Thermal stability for (1-*x*)BNBT-*x*NMS ceramics at 10 kHz. **(b)** PFM amplitude after relaxation of 5 min for 0.84BNBT-0.16NMS ceramic.

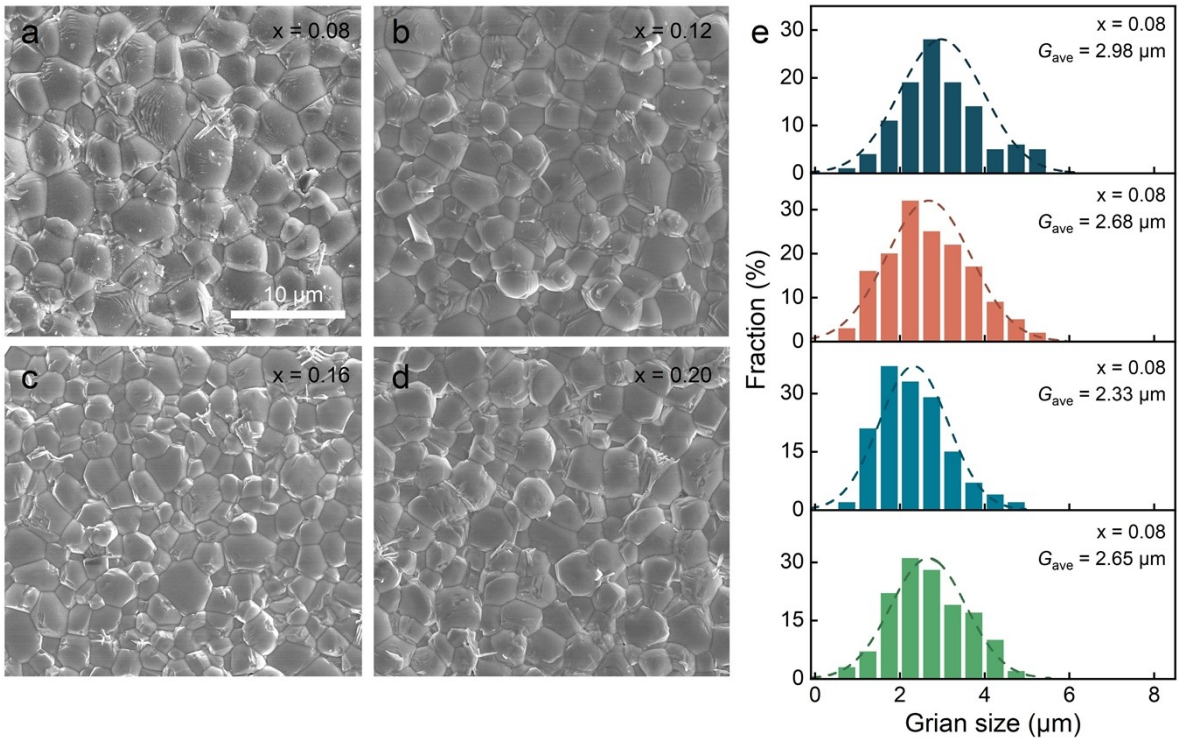

Figure S5 (**a-d**) SEM images of (1-*x*)BNBT-*x*NMS ceramics and (**e**) the corresponding grain size distribution chart.

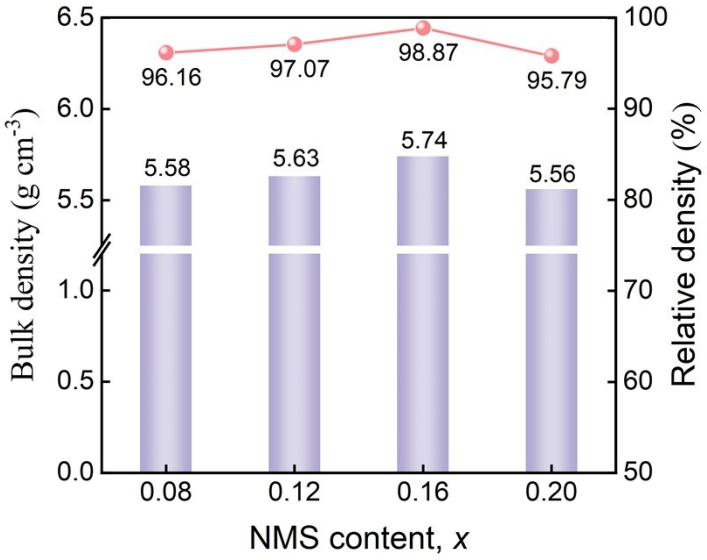

Figure S6 Bulk density and relative density for all ceramics.

Table S1 Refined structural parameters of (1-*x*)BNBT-*x*NMS ceramics.

Component	Space group	Lattice parameters	V (Å^3)
0.08	*R*3*c* (59.14%)	$a = b = 5.52397$, $c = 13.56581$, $\alpha = \beta = 90^\circ$, $\gamma = 120^\circ$	358.493
	*P*4*bm* (40.86%)	$a = b = 5.51595$, $c = 3.90227$, $\alpha = \beta = \gamma = 90^\circ$	118.730
0.12	*R*3*c* (43.52%)	$a = b = 5.52803$, $c = 13.54702$, $\alpha = \beta = 90^\circ$, $\gamma = 120^\circ$	358.522
	*P*4*bm* (56.48%)	$a = b = 5.51561$, $c = 3.90261$, $\alpha = \beta = \gamma = 90^\circ$	118.725
0.16	*R*3*c* (20.27%)	$a = b = 5.51783$, $c = 13.54925$, $\alpha = \beta = 90^\circ$, $\gamma = 120^\circ$	357.259
	*P*4*bm* (79.73%)	$a = b = 5.51597$, $c = 3.90233$, $\alpha = \beta = \gamma = 90^\circ$	118.732
0.20	*R*3*c* (12.63%)	$a = b = 5.51706$, $c = 13.52013$, $\alpha = \beta = 90^\circ$, $\gamma = 120^\circ$	356.432
	*P*4*bm* (87.37%)	$a = b = 5.51993$, $c = 3.91477$, $\alpha = \beta = \gamma = 90^\circ$	118.991

Table S2 V-F fitting parameters for (1-*x*)BNBT-*x*NMS ceramics.

Component	f_0 (Hz)	T_f (K)	E_a (eV)
$x = 0.08$	8.0×10^{10}	360.6	0.0311
$x = 0.12$	5.0×10^{11}	327.2	0.0844
$x = 0.16$	6.0×10^{11}	280.2	0.1293
$x = 0.20$	1.0×10^{12}	240.7	0.1750

Table S3 The parameters used in the finite element simulations for breakdown behavior.

Parameters	Value	Definition
β	1×10^{10} Vm^5C^-	LGD parameter
Γ_g	3.6×10^{-8} J m^{-1}	Constant coefficient related to the breakdown energy of the grain regions
Γ_{gb}	3.6×10^{-9} J m^{-1}	Constant coefficient related to the breakdown energy of the grain boundary regions
$\varepsilon_g(0)$	796.74	The ε_r of the grain regions in 0.92BNBT-0.08NMS
$\varepsilon_{gb}(0)$	79.674	The ε_r of the grain boundary regions in 0.92BNBT-
$\varepsilon_g(0)$	455.58	The ε_r of the grain regions in 0.84BNBT-0.16NMS
$\varepsilon_{gb}(0)$	45.558	The ε_r of the grain boundary regions in 0.84BNBT-
ε_0	8.854×10^{-12}	Permittivity of space
δ	10^{-4}	A small positive constant meant to numerical stability

References

1. Chaitanya Pitike, K.; Hong, W., Phase-field model for dielectric breakdown in solids. *J. Appl. Phys.* **2014,** *115* (4), 044101.
2. Cai, Z.; Wang, X.; Luo, B.; Hong, W.; Wu, L.; Li, L., Dielectric response and breakdown behavior of polymer-ceramic nanocomposites: The effect of nanoparticle distribution. *Compos. Sci. Technol.* **2017,** *145*, 105-113.
3. Zhao, P.; Cai, Z.; Chen, L.; Wu, L.; Huan, Y.; Guo, L.; Li, L.; Wang, H.; Wang, X., Ultra-high energy storage performance in lead-free multilayer ceramic capacitors via a multiscale optimization strategy. *Energy Environ. Sci.* **2020,** *13* (12), 4882-4890.
4. Johnson, K. M., Variation of dielectric constant with voltage in ferroelectrics and its application to parametric devices. *J. Appl. Phys.* **1962,** *33* (9), 2826-2831.
5. Khondabi, M.; Ahmadvand, H.; Javanbakht, M., Revisiting the Dielectric Breakdown in a Polycrystalline Ferroelectric: A Phase-Field Simulation Study. *Advanced Theory and Simulations* **2022,** *6* (1), 2200314.